First-principles DFT + GW study of oxygen vacancies in rutile TiO_2

Andrei Malashevich,[1,2,3] Manish Jain,[1,2,4] and Steven G. Louie[1,2,*]
[1]*Department of Physics, University of California, Berkeley, California 94720, USA*
[2]*Materials Sciences Division, Lawrence Berkeley National Laboratory, Berkeley, California 94720, USA*
[3]*Department of Applied Physics, Yale University, New Haven, Connecticut 06511, USA*
[4]*Department of Physics, Indian Institute of Science, Bangalore 560012, India*
(Received 14 September 2013; revised manuscript received 24 December 2013; published 18 February 2014)

We perform first-principles calculations of the quasiparticle defect states, charge transition levels, and formation energies of oxygen vacancies in rutile titanium dioxide. The calculations are done within the recently developed combined DFT + GW formalism, including the necessary electrostatic corrections for the supercells with charged defects. We find the oxygen vacancy to be a negative U defect, where U is the defect electron addition energy. For Fermi level values below ∼2.8 eV (relative to the valence-band maximum), we find the +2 charge state of the vacancy to be the most stable, while above 2.8 eV we find that the neutral charge state is the most stable.

DOI: 10.1103/PhysRevB.89.075205 PACS number(s): 61.72.jd, 61.72.Bb, 71.23.An

I. INTRODUCTION

Titanium dioxide (TiO_2) attracts a lot of attention of researchers as a versatile functional material used in numerous technological applications, including photocatalysis, hydrolysis, solar cells, high-k dielectrics, optoelectronic devices, sensors, etc. [1–9]. Lattice defects, such as vacancies, substitution impurities, and interstitial impurities inevitably occur in materials regardless of whether they are synthesized or created naturally. These defects can greatly influence the mechanical, electrical, thermal, and optical properties of solids.

Among the major three crystal polymorphs of TiO_2, rutile is the most common one, the other two being anatase and brookite. Rutile TiO_2 has a tetragonal primitive cell with two formula units (see Fig. 1) and its symmetry is described by the space group $P4_2/mnm$. The lattice parameters are $a = 4.594$ Å and $c = 2.959$ Å at room temperature. The Ti and O atoms reside at the $2a$ and $4f$ Wyckoff positions, the latter characterized by the single internal parameter $u = 0.305$ [10].

Rutile TiO_2 in its stoichiometric form is an insulator with an optical band gap of 3.0 eV [11,12]. The optical gap, however, is smaller than the electronic band gap due to electron-hole interactions. The latter band gap is connected to a single-particle (or quasiparticle) description and can be measured in photoemission experiments. The values for the electronic gap in the literature vary in the range of 3.3–4.0 eV [13–15]. For more discussion on the relation between the electronic and optical gaps of TiO_2, as well as a comparison of experimental and theoretical values, see, e.g., Ref. [16].

Heating rutile crystals in a reducing atmosphere results in an increase of the (n-type) electrical conductivity, and rutile composition changes to nonstoichiometric TiO_{2-x}. This change is attributed to various types of defects such as oxygen vacancies, Ti^{3+} and Ti^{4+} interstitials, and planar defects [2].

In this work, we perform calculations of the charge transition levels and defect formation energies of oxygen vacancies in three charge states following a recently developed DFT + GW approach [17,18]. There are several advantages of this approach over the traditional DFT-only approaches [19]. In this method, the GW correction of DFT eigenvalues takes care of the self-energy and self-interaction errors and resolves the problem of band-gap underestimation. The latter problem is often responsible for an incorrect DFT prediction of the defect level position outside the bulk band gap. In addition, within the DFT + GW approach, the formation energies can be calculated without computing the differences in total energies of systems with a *different* number of electrons. We note that the need to go beyond the standard DFT approaches for calculations of defect formation energies and charge transition levels is now well recognized, as more studies of the electronic structure of oxides based on hybrid functionals and GW perturbation methods appear in the literature. Recently, Peng and collaborators [20] proposed an alternative scheme to calculate defect formation energies by using GW to correct band-edge energies.

The rest of the paper is organized as follows. Section II describes in detail the DFT + GW formalism used in our calculations. Computational details are given in Sec. III. Then the main results are presented in Sec. IV, followed by a summary in Sec. V.

II. METHODS

A. DFT + GW formalism

The DFT + GW approach employed in this work was developed in Refs. [17] and [18]. Here, we will introduce the notations used in the subsequent sections.

We describe the atomic state of a system with a defect in a charge state q (oxygen vacancy V_O^q in our case) by a generalized coordinate $\mathbf{R}$. In general, $\mathbf{R}$ corresponds to an arbitrary configuration, not necessarily an equilibrium configuration. The equilibrium configuration of the defect in a charge state q will be denoted as $\mathbf{R}_q$. One can define [18] the defect formation energy $E_q^f(\mathbf{R},\mu_O,E_F)$, which depends on the chemical potential of oxygen μ_O (determined by the experimental preparation conditions) and the Fermi level E_F. We reference E_F to the valence-band maximum (VBM), so it can take values between zero and the bulk band gap depending on the specific sample.

The charge transition level $\epsilon^{q/q-1}$ is defined as the Fermi level at which the charge state of the defect changes from q to

*sglouie@berkeley.edu

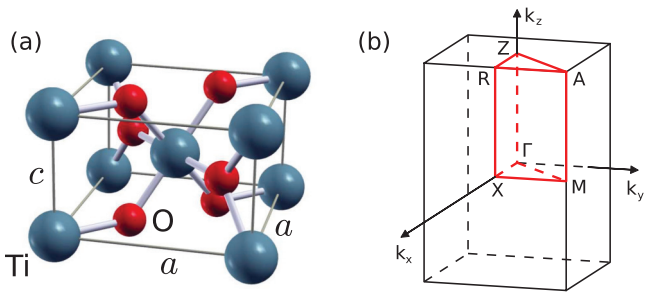

FIG. 1. (Color online) (a) Tetragonal primitive cell of TiO_2 in the rutile crystal structure. (b) The corresponding Brillouin zone.

$q-1$ or, in other words, at which the formation energies of the defect in charge states q and $q-1$ are equal. One can show that the value of the charge transition level can be separated into two contributions as $\epsilon^{q/q-1} = E_{\rm relax} + E_{\rm QP}$, where $E_{\rm QP}$ is a quasiparticle excitation energy (addition or removal of a single electron) and $E_{\rm relax}$ is the (atomic) relaxation energy of the defect in the new charge state. Since $E_{\rm relax}$ is given by the difference in the total energies of the system whose total number of electrons remains unchanged, it can be calculated accurately using standard DFT methods, while $E_{\rm QP}$ may be evaluated using the *ab initio* GW method [21].

The combined DFT + GW approach avoids the typical problems one encounters when using DFT for all terms, such as the underestimation of the band gap and self-interaction errors.

B. Electrostatic corrections

Ideally, when studying defects, one would like to consider a single defect in an infinite bulk material. In practice, however, one often uses a supercell approach [22], in which a finite supercell with a defect is constructed, and periodic boundary conditions are applied. If the supercell is not large enough, the spurious interactions between the defect and its own images should be taken into account. For charged defects, in particular, the spurious long-range Coulomb potential from defect images results in a shift of the defect state in the bulk band gap. This effect has been shown to be quite significant for oxygen vacancies in hafnia [18].

There are several ways to calculate the electrostatic corrections, to be denoted as $\Delta E_{\rm QP}^{\rm e.s.}$. All of them can be done within the DFT-only formalism since the spurious potential is electrostatic and affects only the Hartree potential in the DFT calculation. Furthermore, the Hartree potential is not affected by the self-energy operator within our GW approach. The straightforward approach would be to increase the size of the supercell with a defect and keep track of the shift in the Kohn-Sham eigenvalue corresponding to the defect state. Taking into account the fact that the strength of the Coulomb interaction is inversely proportional to the distance, one can extrapolate the change in the Kohn-Sham eigenvalue to infinite supercell size [18]. This approach, however, requires construction of supercells with a very large number of atoms (often thousands of atoms are required).

In this work, we opted for a different approach proposed by Freysoldt and collaborators [23], which does not require the construction of extremely large supercells. The only requirement on the supercell size is that the charge density associated with the defect state is well localized in a small volume inside the supercell. In the following, we describe the main changes to this method adapting it to DFT + GW framework. We shall keep the original notations and definitions.

If a neutral defect state can be described by a local wave function $\psi_{\rm d}$, then one can calculate the *unscreened* charge density $q_{\rm d}(\mathbf{r})$ associated with the *charged* defect (assuming the charge q goes entirely to the local defect state). The charge q then becomes screened by the surrounding electrons. The corresponding change in the electrostatic potential relative to the neutral defect is denoted by $V_{q/0}$. Note that in this discussion, as in the original formulation [23], we do not consider the effects of lattice relaxations due to the change of the charge state of the defect.

Now we consider a periodic system corresponding to an array of charged defects and add a compensating homogeneous background charge with density $n = -q/\Omega$, where Ω is the supercell volume. Assuming a linear-response behavior, the change in the electrostatic potential for this system $\widetilde{V}_{q/0}(\mathbf{r})$ is given by a superposition of the potentials $V_{q/0}(\mathbf{r}+\mathbf{R})$ up to a constant, where $\mathbf{R}$ denotes lattice vectors. Thus, knowing $V_{q/0}(\mathbf{r})$ of an infinite system, one can reproduce the potential $\widetilde{V}_{q/0}(\mathbf{r})$ of a periodic system (up to a constant). The spurious electrostatic potential induced by the images of the defect in the home supercell is, thus, given by $[\widetilde{V}_{q/0}(\mathbf{r}) - V_{q/0}(\mathbf{r})]$. Within DFT, this corresponds to the undesired shift of the Kohn-Sham defect state,

$$\Delta\epsilon_{\rm d}^{\rm KS} = -\int_{\Omega} d^3r\, |\psi_{\rm d}(\mathbf{r})|^2 [\widetilde{V}_{q/0}(\mathbf{r}) - V_{q/0}(\mathbf{r})]. \quad (1)$$

In practice, we can compute the periodic potential $\widetilde{V}_{q/0}(\mathbf{r})$, but we do not know the original potential $V_{q/0}(\mathbf{r})$ of the infinite system. At large distances, this potential may be well approximated by the long-range screened Coulomb potential [23] $V_{q/0}^{\rm lr}(\mathbf{r})$, which requires knowledge of the dielectric constant ε (which, in turn, can be found, e.g., from density-functional perturbation theory) for its evaluation. Thus, the idea is to separate the potential $V_{q/0}(\mathbf{r})$ into long-range and short-range parts as $V_{q/0}(\mathbf{r}) = V_{q/0}^{\rm lr}(\mathbf{r}) + V_{q/0}^{\rm sr}(\mathbf{r})$. Assuming that the short-range potential decays rapidly with distance and is essentially zero at the border of the supercell (with the defect placed in the center of the supercell), we can write for $\mathbf{r} \in \Omega$

$$\widetilde{V}_{q/0}^{\rm sr}(\mathbf{r}) = V_{q/0}^{\rm sr}(\mathbf{r}) + C, \quad (2)$$

where the constant C absorbs the ambiguity in the absolute position of $\widetilde{V}_{q/0}$. This constant may be found by requiring that $\widetilde{V}_{q/0}$ and $\widetilde{V}_{q/0}^{\rm lr}$ align far from the defect.

Hence, the shift of the defect state due to the spurious electrostatic potential, Eq. (1), can be calculated from two parts, each coming from the long-range and short-range contributions to the potential. The first part is given by

$$\Delta\epsilon_{\rm d,lr}^{\rm KS} = -\int_{\Omega} d^3r\, |\psi_{\rm d}(\mathbf{r})|^2 \left[\widetilde{V}_{q}^{\rm lr}(\mathbf{r}) - V_{q}^{\rm lr}(\mathbf{r})\right] \quad (3)$$

and the second part is given by

$$\Delta\epsilon_{\rm d,sr}^{\rm KS} = -\int_{\Omega} d^3r\, |\psi_{\rm d}(\mathbf{r})|^2 \left[\widetilde{V}_{q/0}^{\rm sr}(\mathbf{r}) - V_{q/0}^{\rm sr}(\mathbf{r})\right] = -C. \quad (4)$$

Equations (3) and (4) give the spurious *shift* of the Kohn-Sham level, while the electrostatic correction $\Delta E_{\mathrm{QP}}^{\mathrm{e.s.}}$ that needs to be applied is

$$\Delta E_{\mathrm{QP}}^{\mathrm{e.s.}} = -\Delta\epsilon_{\mathrm{d,lr}}^{\mathrm{KS}} - \Delta\epsilon_{\mathrm{d,sr}}^{\mathrm{KS}}. \quad (5)$$

To see how the above-described method works, we performed a calculation of the oxygen vacancy in rocksalt MgO in its +1 charge state. For simplicity, we performed a spin unpolarized calculation using a $2 \times 2 \times 2$ cubic supercell (63 atoms). We found a Kohn-Sham eigenvalue in the bulk band gap corresponding to a defect state located 1.07 eV above the VBM. The electrostatic correction calculated with the above method resulted in a shift of the defect eigenvalue of −0.65 eV, where −0.45 eV comes from the first term in Eq. (5) and −0.20 eV comes from the second term. Then, we performed calculations using $3 \times 3 \times 3$ (215 atoms) and $4 \times 4 \times 4$ (511 atoms) supercells. We found the defect eigenvalue to be 0.83 and 0.64 eV above the VBM in 215-atom and 511-atom supercells, respectively. We fit the defect eigenvalue to $\epsilon_d = \epsilon_d^0 + A/L$, where L is the size of the supercell in arbitrary units (e.g., $L = 2,3,4$ in our case), and ϵ_d^0 and A are fitting parameters. In this way, in the limit of an infinite supercell, we found the electrostatic correction to be −0.84 eV, which is in reasonable agreement with the previous result.

Recently, a similar procedure for correcting the Kohn-Sham eigenvalues due to electrostatic spurious potential was suggested by Chen and Pasquarello [24].

III. COMPUTATIONAL DETAILS

In this work, all mean-field calculations were done within the density functional theory framework. It has been shown recently that structural relaxation in the case of rutile TiO_2 depends strongly on the choice of exchange-correlation potential [25]. An adequate description of the crystal structure can be obtained using hybrid functionals, such as that of Heyd, Scuseria, and Ernzerhof (HSE) [26]. If the crystal structure of rutile TiO_2 with oxygen vacancy is relaxed, e.g., using the Perdew, Burke, and Ernzerhof (PBE) exchange-correlation potential [27], the defect level moves into the conduction band regardless of its charge state [25]. For this reason, in our work, all structural relaxations (both for bulk TiO_2 and supercells with defects) were performed using the HSE06 hybrid functional [26], in which 25% of the (short-range) Hartree-Fock (HF) exchange is mixed with 75% PBE exchange. We used the projector augmented-wave (PAW) method [28,29] as implemented in the VASP code package [30]. The standard PBE pseudopotentials for both Ti and O supplied with the VASP package were employed. For Ti, the $3s$, $3p$, $3d$, and $4s$ states were treated as valence orbitals. We used a plane-wave basis set with an energy cutoff of 450 eV.

For bulk TiO_2, the Brillouin zone was sampled by a uniform $4 \times 4 \times 6$ k-point mesh. Oxygen vacancies were simulated by constructing a $2 \times 2 \times 3$ supercell of 72 atoms and removing one O atom. Brillouin zone integrations for the supercells were performed using an equivalent $2 \times 2 \times 2$ mesh of k points.

Once the structural parameters for a system of interest were determined, we performed a separate self-consistent-field (SCF) calculation using the PBE exchange-correlation potential in order to obtain a mean-field starting point for our GW calculations. For this purpose, we used the QUANTUM ESPRESSO code package [31]. Troullier-Martins norm-conserving pseudopotentials [32] were generated for Ti and O. For Ti, the $3s$ and $3p$ semicore states were treated as valence states and the pseudopotential was generated in the Ti^{4+} configuration. The cutoff radii for the $3s$, $3p$, and $3d$ states were chosen to be 0.9, 0.9, and 1.0 a.u., respectively. The energy cutoff for the plane-wave basis of 200 Ry was used in this case.

The GW calculations were performed using the BerkeleyGW code package [21,33]. We used a G_0W_0 approach within the complex generalized plasmon-pole (GPP) model [34]. For the dielectric matrix calculation, the frequency cutoff was chosen to be 40 Ry and the number of valence and conduction bands was chosen to be 2000 for bulk rutile TiO_2 and 4000 for the supercell calculations. In the case of supercells, the convergence with respect to empty states is not guaranteed despite the large number of states used in our calculations. For this reason, the extrapolation to an infinite number of states is required. We used the static-remainder method for this purpose [35].

IV. RESULTS

A. Bulk rutile TiO_2

The structural properties of bulk rutile TiO_2 were calculated using both PBE and HSE06 exchange-correlation potentials. The results of these calculations are in very good agreement with each other and with experiment, as can be seen from Table I.

The electronic band structure was computed along high symmetry lines [the labels for the high symmetry points in the Brillouin zone are shown in Fig. 1(b)]. The band-structure plots before and after the self-energy correction are shown in Fig. 2. As one can see from the figure, the effect of the G_0W_0 correction to a first approximation can be considered as a scissor-shift operation, although the corrections to some bands are larger than to the others.

Within PBE, the calculated band gap is a direct gap of only 1.86 eV at the Γ point. After applying the GW correction, we found the fundamental gap to be the indirect Γ-R gap of 3.13 eV, although the direct gap at the Γ point of 3.18 eV is very close to the Γ-R gap. A more detailed analysis of the band structure of bulk rutile TiO_2, including the calculation of quasiparticle effective masses, is given in the Supplemental Material [36].

TABLE I. Calculated and experimental structural parameters of rutile TiO_2.

	a (Å)	c/a	u
PBE	4.64	0.639	0.305
HSE06	4.58	0.646	0.305
Expt.[a]	4.59	0.644	0.305

[a]Reference [10].

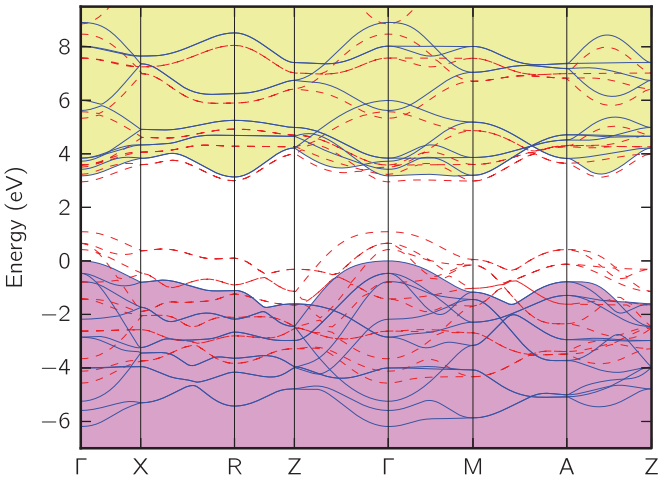

FIG. 2. (Color online) Theoretical band structure of rutile TiO_2 calculated within DFT using the PBE exchange-correlation potential (red dotted lines) and using the GW method (blue solid lines).

B. Oxygen vacancy

Qualitatively, the important defect state in the gap associated with the oxygen vacancy in rutile TiO_2 can be understood as follows. In bulk rutile TiO_2, each O atom is surrounded by three neighboring Ti atoms. When one O atom is removed, the three Ti dangling bonds (mostly having d character) form a low-energy state of a_1 symmetry [25]. In the neutral charge state of the oxygen vacancy (V_O^0), the defect state a_1 is doubly occupied. In the $+1$ charge state (V_O^+), the a_1 is singly occupied. In both cases, the occupied a_1 state bonds the neighboring Ti atoms and keeps them from moving away from the vacancy. In the $+2$ charge state (V_O^{2+}), the a_1 state is unoccupied, which results in much larger displacements of the Ti atoms outward from the vacancy site.

It is worth noting that if one simply relaxes the 0 or $+1$ charged systems within PBE, one may find a ground state which does not necessarily correspond to the electrons bound to the vacancy site. Recently, first-principles calculations [37–39] have shown that polarons may form in TiO_2. In addition, experimental evidence of intrinsic polarons in rutile TiO_2 has been seen in electron paramagnetic resonance measurements [40]. Indeed, in our calculations we find that a naive relaxation of the $+1$ charged system leads to a ground state with an electron away from the vacancy site. We find a localized state with its eigenvalue in the gap, but the charge density corresponding to this state is not localized at the vacancy site but is localized at the next-nearest-neighbor Ti atom. While in principle a polaron can be formed anywhere in the supercell, its localization on the next-nearest Ti atom can be attributed to the finite size of the supercell used in our calculations. Figure 3(a) shows the calculated charge density of the state in the gap for such a polaron ground state. However, for the purpose of calculation of charge transition levels, this particular state is not appropriate. To stabilize the $+1$ vacancy state of interest (i.e., the electron bound to the vacancy site), we used the following procedure. First, we performed a spin-unpolarized relaxation of the neutral vacancy. This resulted in a state with two electrons bound to the vacancy site. Second, we relaxed the $+1$ charged system starting from the atomic configuration found in the first step. This procedure ensured that the defect state remained bound to the vacancy site. Figure 3(b) shows the charge density of the obtained $+1$ vacancy defect state. We emphasize again that the state thus found is not a ground state (i.e., lowest total energy) in our calculations but rather a local minimum. We found that it is above the ground state (we call it a polaron ground state) by 1.2 eV.

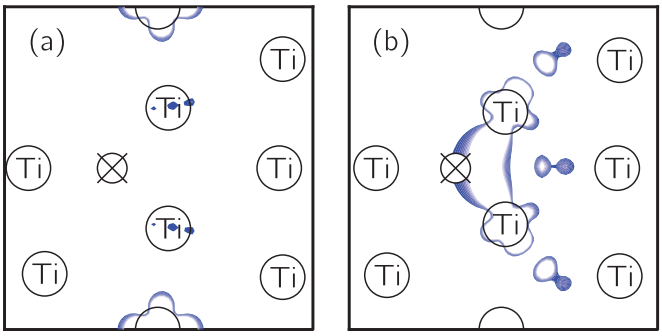

FIG. 3. (Color online) Charge densities of the localized states in the gap found in the HSE calculations with $+1$ charged supercells. Panel (a) shows the ground state, corresponding to a $+2$ charged oxygen vacancy and a polaron. Panel (b) shows the $+1$ charged oxygen vacancy. The isosurfaces show 10% of the charge densities of the localized states.

For the purpose of doing the GW calculation, we used a PBE mean-field solution from a structure determined with HSE. This was done because GW calculation requires a large number of empty bands, and the computational cost of using HSE as the mean field becomes prohibitive. This is a reasonable procedure because GW is a perturbative correction and does not depend sensitively on the starting mean field. Because our GW calculation is a G_0W_0 calculation, we ensured that the resulting PBE defect wave function is similar to the one obtained from HSE. Figure 4 shows the charge density from the defect wave function obtained within PBE.

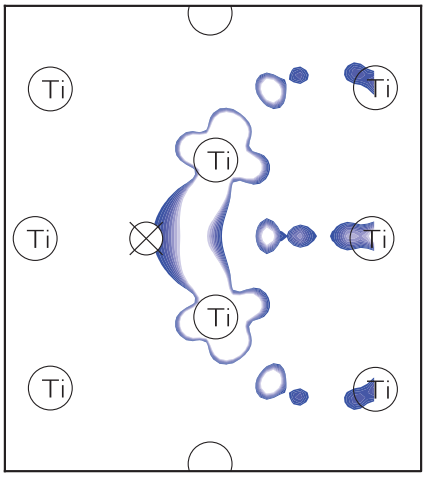

FIG. 4. (Color online) Charge density of the localized defect state of the $+1$ charged oxygen vacancy found in the PBE calculation. The isosurface shows 10% of the charge density. The atomic positions are the same as in Fig. 3(b).

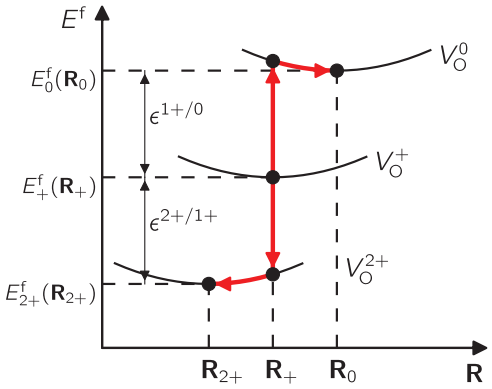

FIG. 5. (Color online) Schematic illustration of the calculation of the charge transition levels $\epsilon^{2+/1+}$ and $\epsilon^{1+/0}$ within the DFT + GW formalism. Arrows indicate the actual paths used in our calculations.

Comparing this figure to Fig. 3(b), we can see that the defect state charge densities obtained using PBE and HSE for the same structure are similar.

To calculate the charge transition levels, we started from +1 charged oxygen vacancy. Figure 5 schematically illustrates the paths in formation energy versus generalized coordinate space that we took. It has been shown that all paths in this space give the same value of charge transition levels to within ±0.1 eV provided that electrostatic corrections are taken into account [18]. To reduce the computational cost, we performed GW calculation on the +1 charged oxygen vacancy. This allows us to calculate both $\epsilon^{1+/0}$ and $\epsilon^{2+/1+}$ as can be seen from Fig. 5. For $\epsilon^{1+/0}$ we computed the quasiparticle (quasielectron) energy of the lowest unoccupied localized state (which in our case turned out to be slightly above the CBM). For $\epsilon^{2+/1+}$ we computed the quasiparticle (quasihole) energy of the +1 defect state. Both quasiparticle energies were evaluated relative to the valence-band maximum E_v, since we defined $\epsilon^{q/q-1}$ relative to E_v in Sec. II A.

Table II shows the results of our computed quasiparticle and relaxation energies as well as the corresponding charge transition levels. From the table, it is clear that the oxygen vacancies are negative U defects, where U is the defect charging energy. Also from the table, one can see that electrostatic corrections are not negligible and have to be included in the calculation.

Furthermore, one can calculate the absolute formation energies as a function of Fermi energy. For a given chemical potential of oxygen, one needs to know the formation energy of the neutral vacancy, which can be calculated within DFT, since

TABLE II. Contributions to the charge transition levels coming from the quasiparticle energy E_{QP}, relaxation energy E_{relax}, and electrostatic correction $\Delta E^{e.s.}_{QP}$ (all values are given in eV).

	$\epsilon^{2+/1+}$	$\epsilon^{1+/0}$
E_{QP}	2.58	3.24
E_{relax}	0.86	−0.29
$\Delta E^{e.s.}_{QP}$	−0.44	−0.44
$\epsilon^{q/q-1}$	3.00	2.51

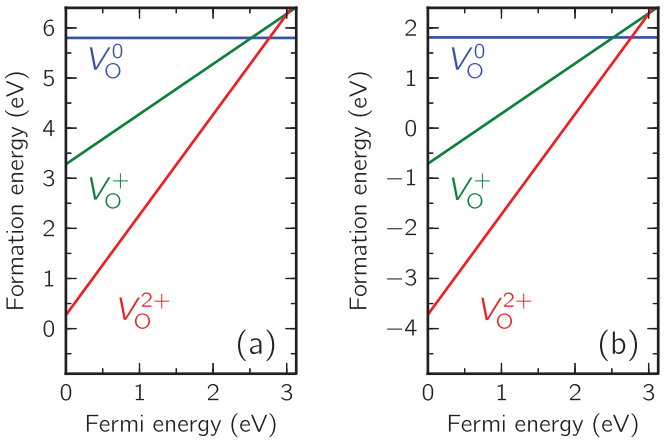

FIG. 6. (Color online) Calculated formation energies of oxygen vacancies in rutile TiO_2 plotted as functions of Fermi level E_F in the (a) oxygen-rich and (b) titanium-rich growth conditions.

for $q = 0$ the absolute values of Kohn-Sham levels do not enter in the definition of formation energy [18]. Note also that the formation energy of the neutral vacancy does not depend on the value of the Fermi level E_F. Then using the definition of charge transition levels, one can obtain the formation energy for all the charge states for a given chemical potential of oxygen. Namely, for a +1 oxygen vacancy V_O^+, one can write

$$E^f_{1+}(E_F) = E^f_0 - \epsilon^{1+/0} + E_F, \quad (6)$$

while a corresponding relation for V_O^{2+} is

$$E^f_{2+}(E_F) = E^f_0 - \epsilon^{1+/0} - \epsilon^{2+/1+} + 2E_F. \quad (7)$$

It is worth noting that calculating the formation energies of the charged defects in this manner does not involve the value of the valence-band maximum within mean field. This ensures that the energy scale for the electrons is set only by the GW calculation and not by DFT calculations.

Figure 6 shows our results for the formation energy of various charged states of the oxygen vacancy plotted as a function of Fermi energy E_F in the oxygen-rich [Fig. 6(a)] and oxygen-poor [Fig. 6(b)] growth conditions. For oxygen-rich growth conditions, the oxygen chemical potential is $\mu_O = 0$. In the titanium-rich (oxygen-poor) limit, μ_O is determined by the formation of Ti_2O_3, which implies the condition $2\mu_{Ti} + 3\mu_O = \Delta H_f(Ti_2O_3)$. Here $\Delta H_f(Ti_2O_3)$ is the formation enthalpy of Ti_2O_3, which we found to be −15.33 eV (per formula unit). On the other hand, the stability condition for TiO_2 requires $\mu_{Ti} + 2\mu_O = \Delta H_f(TiO_2)$, where the formation enthalpy $\Delta H_f(TiO_2) = -9.66$ eV (per formula unit). From these two conditions we find the oxygen chemical potential to be $\mu_O = -3.99$ eV in the titanium-rich limit.

As can be seen from Fig. 6, the most stable defects in the wide range of possible values for Fermi energy are +2 charged oxygen vacancies. This finding is in qualitative agreement with the previous HSE study by Janotti *et al.* (see Fig. 5 of Ref. [25]). Similar to that work, we also find that the transition from the +2 to the neutral state occurs at a higher value of E_F than the transition from the neutral to the +1 state (a feature of the negative U defect). Quantitatively, however, our values for charge transition levels are smaller than what was

found in Ref. [25] by ∼0.5 eV. To be more precise, charge transition levels in that work were found to be at or above the conduction-band minimum, and, as a result, the V_O^{+2} was found to be the only stable oxygen vacancy for all values of E_F. In our case, we find that for $E_F > 2.8$ eV the neutral vacancy can become more stable.

We emphasize that the study of formation energies and the relative stability of charged oxygen vacancies in rutile TiO_2 cannot be done at the PBE level since in this case the defect levels are not found in the bulk band gap. Therefore, it is crucial to use more advanced methods, such as, e.g., the one described above.

V. SUMMARY

In summary, we investigated the oxygen vacancies in rutile TiO_2 in three charge states from first principles using the DFT + GW approach. The oxygen vacancies were emulated in a 71-atom supercell. The structural relaxations around the defects were performed using the hybrid functional (HSE) method, and charge transition levels and defect formation energies were calculated within the DFT + GW formalism. According to our calculations, in a wide range of values for Fermi energy, $0 < E_F < 2.8$ eV, the +2 charge state of the vacancy is the most stable, while for Fermi energies above 2.8 eV the neutral vacancy is stabilized. This result also means that the oxygen vacancy is found to be a negative U defect.

ACKNOWLEDGMENTS

This work was supported by National Science Foundation Grant No. DMR10-1006184 (ground-state and structural studies, electrostatic correction analyses, and effective mass calculations) and the Theory Program at the Lawrence Berkeley National Laboratory (LBNL) funded by the Department of Energy (DOE), Office of Basic Energy Sciences, under Contract No. DE-AC02-05CH11231 (quasiparticle calculations and studies of charge transition levels). Algorithm developments for large-scale GW simulations were supported through the Scientific Discovery through Advanced Computing (SciDAC) Program on Excited State Phenomena in Energy Materials funded by DOE, Office of Basic Energy Sciences and of Advanced Scientific Computing Research, under Contract No. DE-AC02-05CH11231 at LBNL. S.G.L. acknowledges the support of a Simons Foundation Fellowship in Theoretical Physics. Computational resources have been provided by DOE at Lawrence Berkeley National Laboratorys NERSC facility and by National Institute for Computational Sciences. We would like to thank A. Janotti for helpful discussions.

[1] F. A. Grant, Rev. Mod. Phys. **31**, 646 (1959).
[2] U. Diebold, Surf. Sci. Rep. **48**, 53 (2003).
[3] J. Augustynski, Electrochim. Acta **38**, 43 (1993).
[4] A. L. Linsebigler, G. Lu, and J. T. Yates, Jr., Chem. Rev. **95**, 735 (1995).
[5] B. O'Regan and M. Grätzel, Nature (London) **353**, 737 (1991).
[6] J. J. Yang, M. D. Pickett, X. Li, D. A. A. Ohlberg, D. R. Stewart, and R. S. Williams, Nat. Nanotech. **3**, 429 (2008).
[7] S. K. Kim, G.-J. Choi, S. Y. Lee, M. Seo, S. W. Lee, J. H. Han, H.-S. Ahn, S. Han, and C. S. Hwang, Adv. Mater. **20**, 1429 (2008).
[8] G. D. Wilk, R. M. Wallace, and J. M. Anthony, J. Appl. Phys. **89**, 5243 (2001).
[9] A. Fujishima and K. Honda, Nature (London) **238**, 37 (1972).
[10] S. C. Abrahams and J. L. Bernstein, J. Chem. Phys. **55**, 3206 (1971).
[11] D. C. Cronemeyer, Phys. Rev. **113**, 1222 (1959).
[12] A. Amtout and R. Leonelli, Phys. Rev. B **51**, 6842 (1995).
[13] Y. Tezuka, S. Shin, T. Ishii, T. Ejima, S. Suzuki, and S. Sato, J. Phys. Soc. Jpn. **63**, 347 (1994).
[14] P. J. Hardman, G. N. Raikar, C. A. Muryn, G. van der Laan, P. L. Wincott, G. Thornton, D. W. Bullett, and P. A. D. M. A. Dale, Phys. Rev. B **49**, 7170 (1994).
[15] S. Rangan, S. Katalinic, R. Thorpe, R. A. Bartynski, J. Rochford, and E. Galoppini, J. Phys. Chem. C **114**, 1139 (2010).
[16] L. Chiodo, J. M. García-Lastra, A. Iacomino, S. Ossicini, J. Zhao, H. Petek, and A. Rubio, Phys. Rev. B **82**, 045207 (2010).
[17] M. Hedström, A. Schindlmayr, G. Schwarz, and M. Scheffler, Phys. Rev. Lett. **97**, 226401 (2006); P. Rinke, A. Janotti, M. Scheffler, and C. G. Van de Walle, *ibid.* **102**, 026402 (2009).
[18] M. Jain, J. R. Chelikowsky, and S. G. Louie, Phys. Rev. Lett. **107**, 216803 (2011).
[19] H. Iddir, S. Öğüt, P. Zapol, and N. D. Browning, Phys. Rev. B **75**, 073203 (2007).
[20] H. Peng, D. O. Scanlon, V. Stevanovic, J. Vidal, G. W. Watson, and S. Lany, Phys. Rev. B **88**, 115201 (2013).
[21] M. S. Hybertsen and S. G. Louie, Phys. Rev. B **34**, 5390 (1986).
[22] M. L. Cohen, M. Schlüter, J. R. Chelikowsky, and S. G. Louie, Phys. Rev. B **12**, 5575 (1975).
[23] C. Freysoldt, J. Neugebauer, and C. G. Van de Walle, Phys. Rev. Lett. **102**, 016402 (2009).
[24] W. Chen and A. Pasquarello, Phys. Rev. B **88**, 115104 (2013).
[25] A. Janotti, J. B. Varley, P. Rinke, N. Umezawa, G. Kresse, and C. G. Van de Walle, Phys. Rev. B **81**, 085212 (2010).
[26] J. Heyd, G. E. Scuseria, and M. Ernzerhof, J. Chem. Phys. **118**, 8207 (2003); **124**, 219906(E) (2006).
[27] J. P. Perdew, K. Burke, and M. Ernzerhof, Phys. Rev. Lett. **77**, 3865 (1996).
[28] P. E. Blöchl, Phys. Rev. B **50**, 17953 (1994).
[29] G. Kresse and D. Joubert, Phys. Rev. B **59**, 1758 (1999).
[30] G. Kresse and J. Furthmüller, Phys. Rev. B **54**, 11169 (1996); Comput. Mater. Sci. **6**, 15 (1996).
[31] P. Giannozzi, S. Baroni, N. Bonini, M. Calandra, R. Car, C. Cavazzoni, D. Ceresoli, G. L. Chiarotti, M. Cococcioni, I. Dabo, A. Dal Corso, S. de Gironcoli, S. Fabris, G. Fratesi, R. Gebauer, U. Gerstmann, C. Gougoussis, A. Kokalj, M. Lazzeri, L. Martin-Samos, N. Marzari, F. Mauri, R. Mazzarello, S. Paolini, A. Pasquarello, L. Paulatto, C. Sbraccia, S. Scandolo, G. Sclauzero, A. P. Seitsonen, A. Smogunov, P. Umari, and R. M. Wentzcovitch, J. Phys.: Condens. Matter **21**, 395502 (2009).

[32] N. Troullier and J. L. Martins, Phys. Rev. B **43**, 1993 (1991).
[33] J. Deslippe, G. Samsonidze, D. A. Strubbe, M. Jain, M. L. Cohen, and S. G. Louie, Comput. Phys. Commun. **183**, 1269 (2012).
[34] S. B. Zhang, D. Tománek, M. L. Cohen, S. G. Louie, and M. S. Hybertsen, Phys. Rev. B **40**, 3162 (1989).
[35] J. Deslippe, G. Samsonidze, M. Jain, M. L. Cohen, and S. G. Louie, Phys. Rev. B **87**, 165124 (2013).
[36] See Supplemental Material at http://link.aps.org/supplemental/10.1103/PhysRevB.89.075205 for further details on the calculations of the electronic band structure and quasiparticle effective masses of bulk rutile TiO_2.
[37] P. Deák, B. Aradi, and T. Frauenheim, Phys. Rev. B **83**, 155207 (2011).
[38] P. Deák, B. Aradi, and T. Frauenheim, Phys. Rev. B **86**, 195206 (2012).
[39] A. Janotti, C. Franchini, J. B. Varley, G. Kresse, and C. G. Van de Walle, Phys. Status Solidi RRL **7**, 199 (2013).
[40] S. Yang, A. T. Brant, N. C. Giles, and L. E. Halliburton, Phys. Rev. B **87**, 125201 (2013).